

TRIBOLOGICAL INVESTIGATIONS ON LASER IRRADIATED COMPOSITE THIN FILMS PREPARED BY TVA TECHNIQUE

M. LUNGU^{a,b}, I. TISEANU^a, C. POROSNICU^{a*}, C. DOBREA^a, I. JEPU^a,
P. DINCA^{a,b}, A. MARCU^a, C. P. LUNGU^a

^a*National Institute for Lasers, Plasma and Radiation Physics, Magurele, 077125, Romania*

^b*Faculty of Physics, University of Bucharest, Magurele, Romania*

Using thermionic vacuum arc method fusion mixed layers containing tungsten, nichel and iron in fixed and rotated deposition geometries were deposited. X-ray micro-beam fluorescence method was used in order to identify film composition on specific positions on a 320 mm diameter disc holder. The geometrical dependence on a planar substrate using three independent evaporators was studied comparing 2D X-ray micro-beam fluorescence mapping results with theoretical deposition predictions. Tribological investigations have also shown a composition dependent increase of the wearing rate after ps laser irradiation of the samples.

(Received January 8, 2016; Accepted April 15, 2016)

Keywords: Tribology, Mechanical Properties, Thermionic Vacuum Arc, X-ray Fluorescence

1. Introduction

The production of mixed films that simulate re-deposition of materials that may occur in fusion reactors as JET and ITER is of high interest in our days. Production of mixed layers with mechanical and especially tribological characteristics is of great importance for industry [1]. The few micrometer coating of these materials are prepared using the thermionic vacuum arc (TVA) technology [2-3]. Switching the attention towards DEMO [4] in the mixed film deposition field, there are incipient studies concerning layer containing mixed W and metal. During DEMO operation mixed containing W layers will be formed due to erosion and redeposition processes that will occur during the operation, as it happened in JET and it is expected in ITER. It is a great importance to study these mixed materials in a wide range of relative concentrations from the structure and mechanical properties point of view. This paper proposes a method to simulate mixed layers formation of a wide range of concentrations that are characterised by X-ray micro-beam fluorescence (μ XRF) from the point of view of concentration and their tribological properties, investigated before and after a high heat flux (HHF) irradiation performed on these layers. The reason for performing such HHF test is that mixed redeposited layers that will form during DEMO operation will be subject to plasma particles that will not be properly confined by the magnetic field and also be subject to plasma disruptions (ELMs) that induce to these a large amount of energy in a short period of time. This was simulated using a picosecond laser pulse trains with comparable time of operation and injected energies. Tribological and morphological modifications were investigated afterwards.

* Corresponding author: corneliu.porosnicu@inflpr.ro

2. Methods

Using thermionic vacuum arc method mixed films containing W-Fe-Ni were produced using three independent evaporators. Two deposition campaigns were conducted with rotated and fixed geometry. Glass and silicon rectangular substrates of 11 mm x 11 mm were settled on a 320 mm diameter stainless steel probe holder. The distance between the anodes and the sample holder was 210 mm, while the distance between the centers of the probes was kept constant at 19 mm, in total being produced by TVA method a number of 148 samples (Fig. 1).

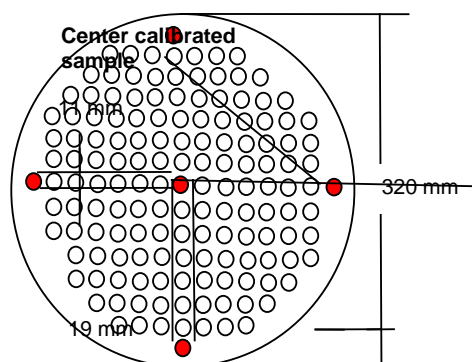


Fig. 1. Dimension specification of probe spatial distribution on sample holder

The composition variation within 1 μm thickness coating layers prepared by TVA method, was analyzed using low value excitation energies (<50 KeV) by the method called micro-beam X-ray fluorescence ($\mu\text{-XRF}$) [5-7]. This method in particular can focus the X-ray beam on the surface of the sample. With this instrument surface mapping of W, Fe and Ni on Silicon were conducted for fixed as for rotated deposition geometry without destroying the deposited surface. This method is optimal for thinner layers deposition less than 5-6 microns due to the saturation effect presented by tungsten L characteristic energetic lines [8]. The measurement standard set-up and samples mounted on the measuring stand are presented in figure 2. From the analysis of X-ray fluorescence spectrum, by determining with calibration samples (bulk Fe, Ni, W) the energy of X-ray peaks, it was possible to qualitatively determine the elemental composition and also to measure the atomic ratio variation on the surface of the samples for both rotated and fixed geometry.

Experimental conditions for $\mu\text{-XRF}$ and source parameters were kept fixed, integration time of 45 seconds, Mo target X-ray source with current of 700 μA and a 45 kV voltage. Using bulk materials, energy calibration of the spectrum was carried out in order to conduct area integration upon characteristic energetic for Fe (K-line 6.39 keV), Ni (K-line 7.47 keV) and W (L-line 8.39 keV). Transformation from integrated peak area to layer thickness was possible in-situ with the use of film thickness monitor based on crystal quartz balance that provided a calibration thickness for the central sample. Ni, W, Fe calibration curves conducted in a prior work shows a linear dependence between the layer thickness and the integrated peak area of photon counts for each element for analyzed samples under 0.5 μm thickness per element [8]. For both deposition setups, within elemental combinations of W-Fe-Ni, a surface mapping campaign was conducted

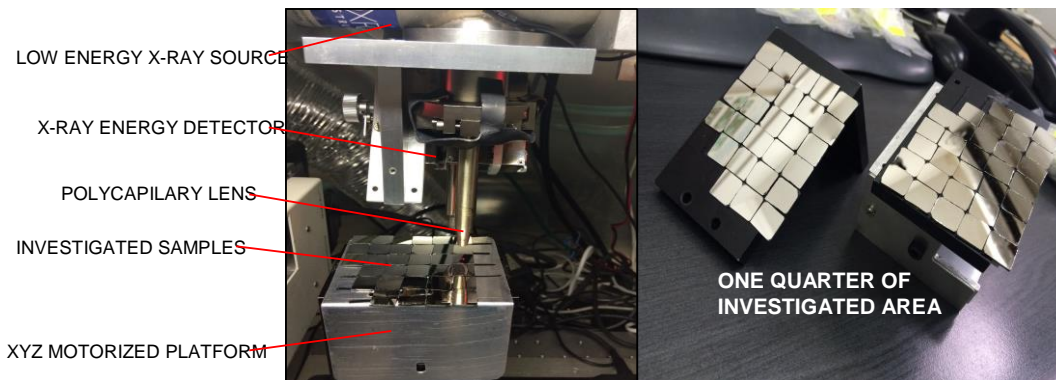


Fig.2 μ -XRF experimental setup with mounted samples(left) and photograph of the analyzed samples - divided area by smaller zones of 55 mm x 66mm (right)

Samples were measured, with a measuring point step of 12 mm (each sample measured once in the center), providing less noise XRF analysis by eliminating the shadowing deposition effect from the margin areas of each probe [8]. The 148 samples on the 320 mm diameter probe holder were placed with a constant gap of 19 mm. In order to fit in the maximum moving area range of the motorized XYZ axis (100 by 100 mm), as shown in Fig.2, we divided in 4 distinct areas (55 by 66 mm).

3. Theoretical considerations on sample preparation

Two cases are investigated. One in fixed geometry, where the substrate holder is kept in the same position during the deposition and the other one when, in order to obtain the same atomic ratios for the three elements, the sample holder is rotated during the entire deposition process. For the setup were the sample holder is rotated around a fixed center in the same plan, 'R' represents the radius between the fixed center and chosen sample point 'S'. The distances between the projection points of the sources (B1, B2, B3) on the sample holder surface and the center of the holder 'O' are x_1 , x_2 respectively x_3 . The height of the pulverization sources are marked with h_1 , h_2 , h_3 and the d_1 , d_2 , d_3 represents the distance from the sample 'R' to the projection points. The last notations are r_1 , r_2 , r_3 that describes the path from the evaporation source to the chosen sample point (S). All notations are presented in Fig. 3 and it could be noticed that x_i , h_i and radius are constant despite the rotation.

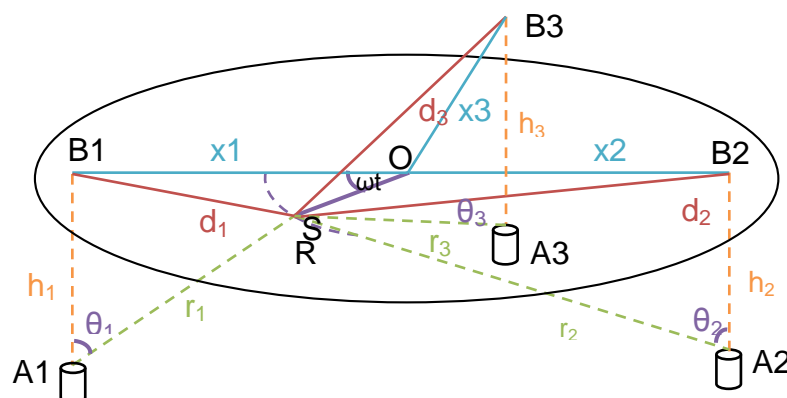


Fig.3 Theoretical deposition modeling for three anode setup of TVA deposition

R_i represent the deposition velocities from Fe, W and Ni sources. In rotational geometry deposition case we have a uniform tendency of deposition along the holder's diameter given by the formula:

$$\int_0^{2\pi} R_i(h_i, x_i, R, \omega t) dt = \alpha_i \frac{h_i^2}{(2x_i R)^2 \omega} \int_0^{2\pi} \frac{d(\omega t)}{\left[\frac{h_i^2 + R^2 + x_i^2}{2x_i R} - \cos(\omega t + \varphi_i) \right]^2} = A \int_{\varphi_i}^{2\pi + \varphi_i} \frac{d(\omega t + \varphi_i)}{[B - \cos(\omega t + \varphi_i)]^2} \quad (1)$$

were A, B are constants, ω represents the angular velocity of the holder, t- time and φ_i the initial angle state. Theoretical distribution was carried out starting with the measurements upon distances (h_i, x_i) in case of Fe anode in the vacuum chamber deposition and with given values for radius from 0 to 150 mm. In Fig.4 black line is showing the result after time integration of the formula (1) for thickness positioned in the centers of the rotating samples.

For the deposition rate in fixed geometry (blue line from Fig.4), it had been applied the equation:

$$deposition\ rate\ (R) = \frac{1}{r_i^2} \cdot \cos\theta_i = \frac{h_i}{(h_i^2 + R^2) \cdot \sqrt{h_i^2 + R^2}} \quad (2)$$

Red line in Fig.4 represents the anode fixed position.

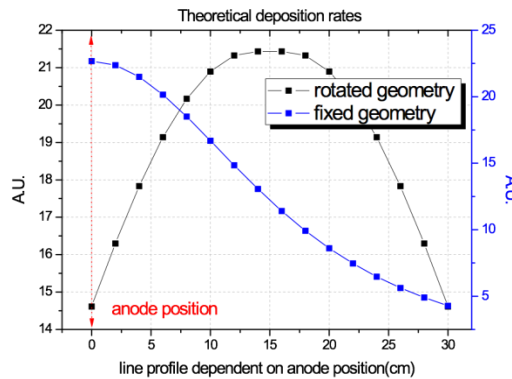


Fig.4 Comparison between theoretical and experimental data distribution obtained for Ni element along the holder's diameter

If the parameters in the eq.4 that were considered fixed (h, X) are varied, we obtain the results from Fig.5 and Fig. 6. Firstly is taken into account the anode height variation at a constant $X=8$ cm (distance from the fixed centre on the holder sample to the anode projection point). In order to have a smooth deposition on the diameter of the sample holder is necessary to have a big distance between the sample holder and the anode (considering the technological constrains of the TVA deposition method). For a better understanding, the right plot from Fig.8 shows the extremities values of anode height curves. In case of the X variation, for a more uniform deposition in a rotated geometry, the higher X value we use, the more uniform the deposited layer results (Fig.6).

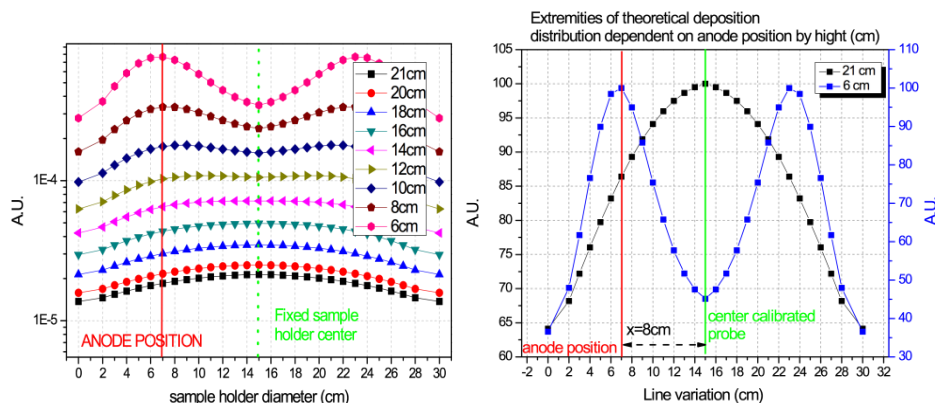


Fig. 5 Deposition uniformity variation dependent on the anode height position

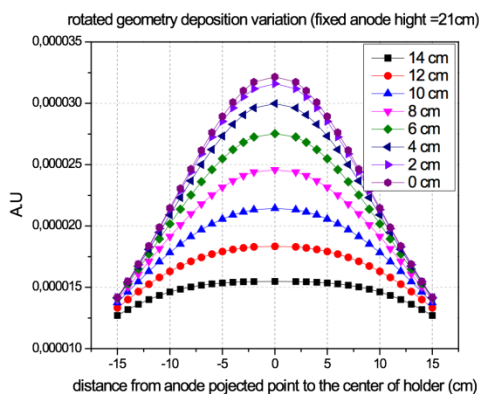


Fig.6 Deposition uniformity variation dependent on the distance from the anode projected point to the fixed centre of sample holder

4. Theory versus measurements

Starting from the Langmuir-Knudsen formula that simulates the deposition rates occurring with the TVA method we can estimate the deposition rate (Fig.7).

$$R_m = 1.85 \cdot 10^{-2} \left(\frac{M}{T}\right)^{1/2} \cos\theta \cos\phi \frac{1}{r^2} [p(T) - p_b] \tag{3}$$

due to the fact that the residual pressure p_b is much smaller than the vapors pressure $p(T)$ and all the samples are in the same samples holder plane ($\theta = \phi$) it results a simplified formula:

$$R_m = 1.85 \cdot 10^{-2} \left(\frac{M}{T}\right)^{1/2} \cos\theta \frac{1}{r^2} [p(T)] \tag{4}$$

The theoretical deposition distribution result after application of eq. 3 for all elements (W, Fe and Ni) is shown by a 3D map surface plot (Fig.7) in arbitrary units.

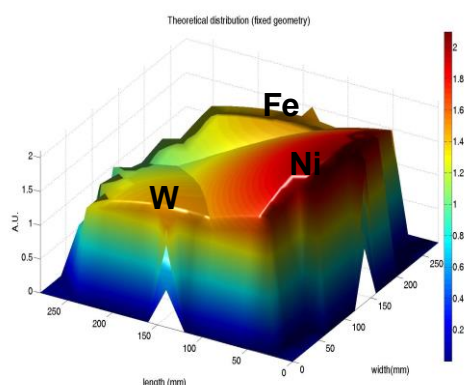


Fig. 7 Color map surface plot in fixed deposition geometry for W, Fe, Ni

Central thickness calibrated probe was analyzed in more than one point in order to make mean values of photon counts correlated to known measured thickness for each deposited element (Fig.8). The recorded values on central probe for fixed geometry (by using film thickness monitor) was W=100 nm, Fe=243 nm and Ni=181 nm with a total deposited thickness of 559 nm. For the rotated geometry deposition the calibrated sample have the values W=101 nm, Fe=244 nm, Ni=181 nm with a total layer thickness of 526nm.

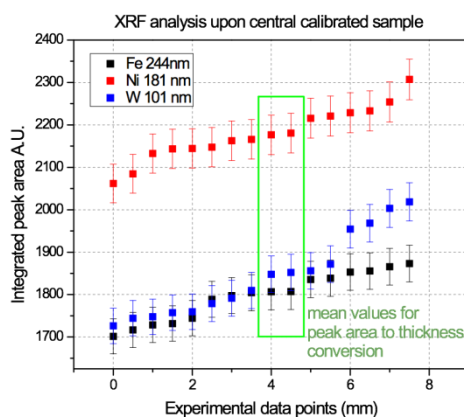


Fig. 8 Central calibrated sample analyzed in multiple central points by μ -XRF method

For comparing the experimental results with the theoretical distributions we make the comparison for a single element, respectively Ni (Fig. 9). In the presented map, the Z axis represents the thickness (nm) converted from the peak area of photon counts using the calibrated central probe, while x and y axis represents the investigated area dimension.

Contour plot shows that the highest deposition thickness is situated as expected above Ni anode area (marked as red area in Fig. 9a) suggesting a higher evaporation rate while the deposition thickness presents a decrease along the line path from the central to periphery, opposite to the Ni anode, (marked as cyan area).

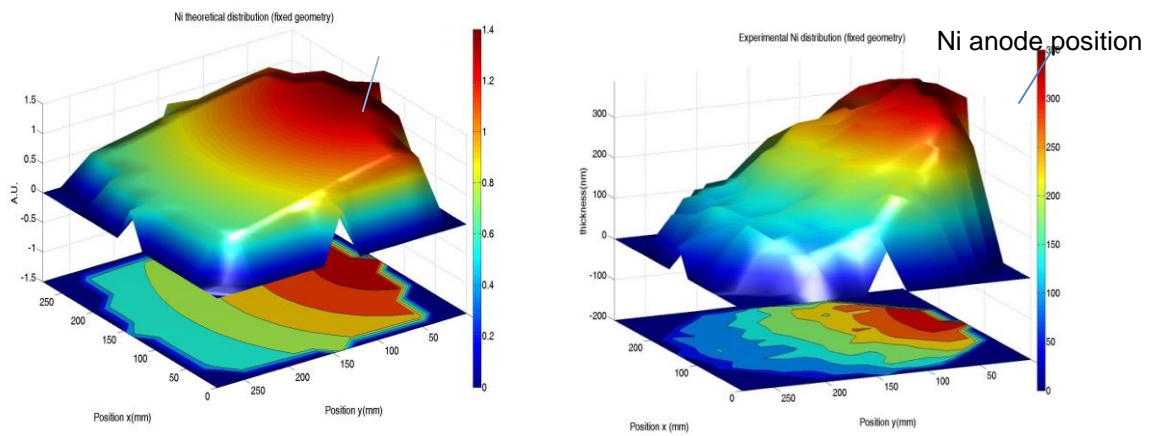


Fig. 9 Experimental / theoretical 3D plot distribution of Ni on sample holder surface

The results are in good agreement with the theoretical results presented in Fig. 9b.

Transforming the Z axis from thickness (nm) to atomic concentration (atoms/cm²) by formula (5).

$$T(nm) \cdot \rho \left(\frac{g}{cm^3} \right) \cdot \frac{N_A \left(\frac{at}{mol} \right)}{M \left(\frac{g}{mol} \right)} = A_c \left(\frac{at}{cm^2} \right) \quad (5)$$

Where the A_c represents the atomic concentration per surface, M – molar mass, N_A Avogadro number (6.022×10^{23}), ρ - element density and T the determined thickness.

The result shown as 3D representation atomic ratio (Fig. 10) was suitable in order for better understanding the elemental deposition variation for the elements constructing the entire layer thickness.

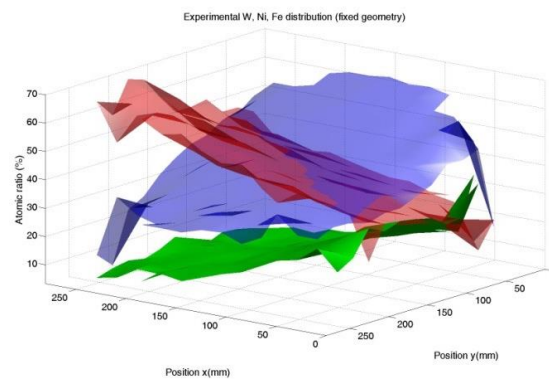


Fig. 10 Atomic ratio of W, Fe, Ni in fixed deposition geometry

μ -XRF experimental line profiles were conducted for the rotated geometry taking into account the theoretical distribution. In order to convert the peak areas into thickness we used the calibrated sample positioned in the fixed center of the sample holder. The results suggest a uniform deposition for all elements, and atomic ratio (Fig. 11) show more clearly a low variation of atomic concentration in the diameter of the sample holder suggesting that by rotation we can achieve an uniform deposition from the relative atomic ratio point of view.

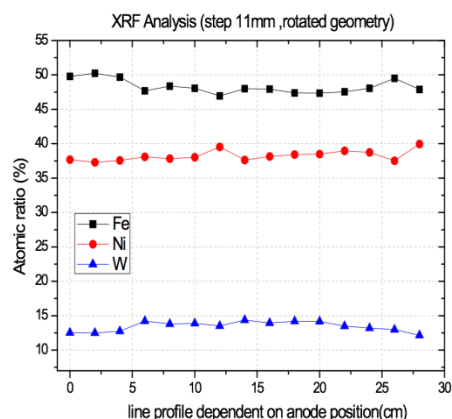


Fig.11 Atomic W-Fe-Ni ratio measured by μ -XRF for the rotated geometry samples

5. Mechanical properties investigations

Tribological measurements were performed to investigate the friction coefficient variation with elemental concentration using a “Ball on disk” tribometer, made by CSM Switzerland, with normal incident forces rated at 0,25 and 0,5N respectively, on a sliding distance of 50 m and linear rate of 2cm/s. The samples were selected so that one of the elemental ratios was kept constant while the other two varied as much as possible.

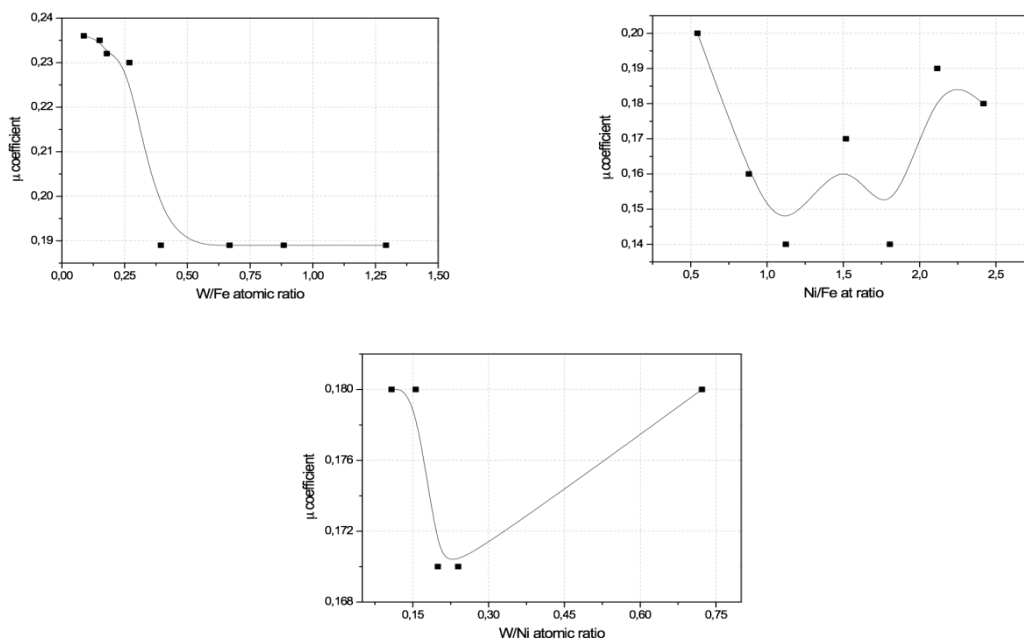


Fig. 12. Friction coefficient variation for the fixed geometry samples, with W/Fe/Ni atomic ratio

A rapid decrease of 0.05, from ~ 0.24 to 0.19 of the friction coefficient is observed when the W/Fe ratio exceeds 0.25. Increasing furthermore the tungsten inside the layer, no significant improvements are observed. For the Ni/Fe and W/Ni ratios, optimum values are observed at intermediary ratios. Between 1 and 2 for Ni/Fe and 0.2 for W/Ni, where the friction coefficient drops below 0.2, a very good value for the dry sliding experiment.

W-Fe-Ni obtained structures by rotating geometry were directly irradiated using a 7ns pulse laser and 355 nm wavelength. There were used 6s length train pulses with 500 000 Khz and

a 3.5 mJ energy per pulse. Even though the beam energy is rather high for this thickness type film, the beam was expanded so that the energy introduced within the film is below the ablation threshold, following only the structural changes. Due to the beam expansion it was obtained a better uniformity of total power density on the sample with a radial symmetry of local energy to which the sample was tested. On the irradiated samples, tribological measurements were performed before and after the exposure using the same conditions mentioned above.

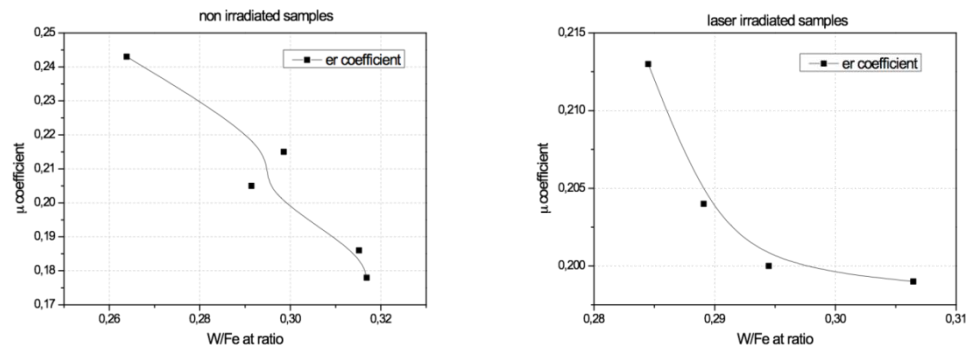


Fig. 13: friction coefficient values for samples with W-Fe-Ni content before (left) and after (right) laser beam direct irradiation

Tribological measurements (Figures 13 and 14) showed a decrease of the friction coefficient between 17 and 33% comparing with its initial values before film irradiation, the variation being due to relative concentrations (W vs. Fe vs. Ni).

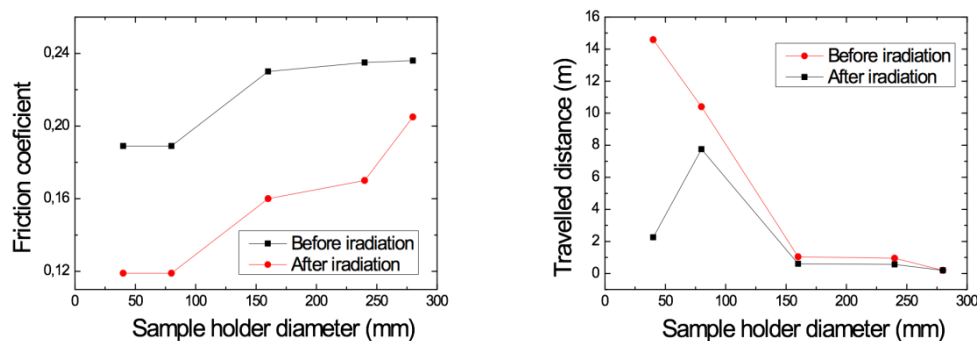


Fig. 14. Friction coefficient value for samples with W-Fe-Ni content before and after laser beam irradiation (left), distance crossed by the stainless steel disk ball during the tribological experiment until film damage

SEM images were acquired for wearing signs after measuring the friction coefficient using tribological methods. As it can be seen in figure 15 and the high wearing rate (the time when the structure is destroyed showed through tribological method) showed that the samples became more brittle after irradiation by cracks with a length of several microns. As the tribological behavior was more obviously improved, the life of structures during the measurements performed for friction coefficient was shortened and the cracks were wider.

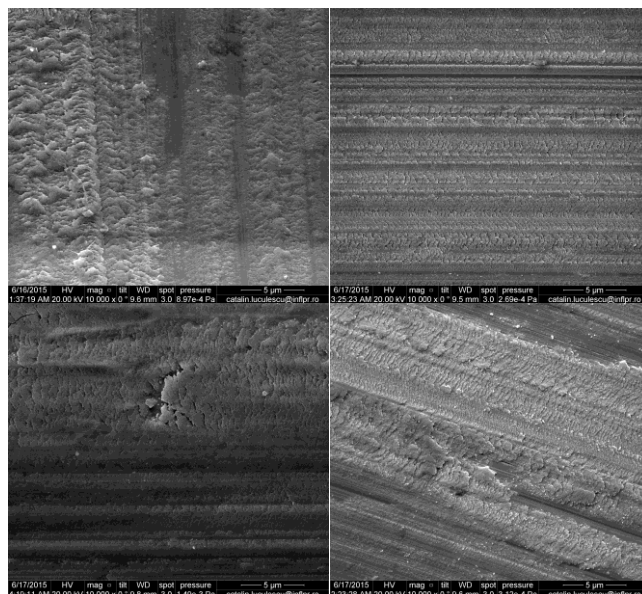


Fig. 15. SEM images for wearing signs after tribological measurements for non-irradiated samples (up) and non-irradiated (down).

6. Conclusions

TVA method is used to produce functional composite materials. The method was optimized using theoretical calculations that were validated by micro-Xray fluorescence method. From the tribologic analysis, the friction coefficient of the ternary structure highly depends on the W/Fe/Ni atomic ratios: increasing the W concentration over Fe, if the Ni ratio remains constant the friction coefficient. Laser irradiation of the layers improve the tribological behavior but decrease their lifetime during dry - sliding tribo-experiments.

Acknowledgements

This work has been financed by the National Authority for Research and Innovation in the frame of Nucleus programme - contract 4N/2016 and supported by two grants of the Romanian National Authority for Scientific Research, CNDI – UEFISCDI, project numbers 80/2014, PN-II-PT-PCCA-2013-4-2165 and 160/2012, PN-II-PT-PCCA-2011-3.2-1453

References

- [1] M.F. Morks, Ivan Cole, Akira Kobayashi, Vacuum, **88**, 134 (2013).
- [2] C. P. Lungu, I. Mustata, V. Zaroschi, A. M.Lungu, A. Anghel, P. Chiru, M. Rubel, P. Coad G. F. Matthews and JET-EFDA contributors, , *Phys. Scr.*, **T128**, 157 (2007).
- [3] C. Porosnicu, A. Anghel, K. Sugiyama, K. Krieger, J. Roth, C.P. Lungu, J. Nuc. Mat. **415**, S713 (2011).
- [4] K. Tobita, et al. Nucl. Fusion **49**, 075029 (2009)
- [5] I. Tiseanu, T. Craciunescu, A. Möslang Fusion Engineering and Design, **84**, 1847 (2009).
- [6] I. Tiseanu, T. Craciunescu, B. Pegourier, H. Maier, C. Ruset, M. Mayer, C. Dobrea, A. Sima, Phys. Scr. T **145**, 014073 (2011).
- [7] I. Tiseanu, M. Mayer, T. Craciunescu, A. Hakola, S. Koivuranta, J. Likonen, C. Ruset, C. Dobrea, ASDEX Upgrade Team, Surface & Coatings Technology **205**, S192 (2011)
- [8] M. Lungu, C. Dobre, T.Craciunescu, I. Tiseanu, C. Porosnicu, I. Jepu, I. Mustata, Digest Journal of Nanomaterials and Biostructures **9**(3), 899 (2014).